Chimica Techno Acta
published by Ural Federal University
eISSN 2411-1414; chimicatechnoacta.ru

ARTICLE
2022, vol. 9(4), No. 20229418
DOI: 10.15826/chimtech.2022.9.4.18

Hydrothermal synthesis and sorption performance to Cs(I) and Sr(II) of zirconia-analcime composites derived from coal fly ash cenospheres

Tatiana A. Vereshchagina [a*], Ekaterina A. Kutikhina [a], Olga V. Buyko [b], Alexander G. Anshits [a,c]

a: Institute of Chemistry and Chemical Technology, Federal Research Center "Krasnoyarsk Science Center of Siberian Branch of the Russian Academy of Sciences", Krasnoyarsk 660036, Russia
b: Research Department, Siberian Federal University, Krasnoyarsk 660041, Russia
c: Department of Chemistry, Siberian Federal University, Krasnoyarsk 660041, Russia
* Corresponding author: vereschagina.ta@icct.krasn.ru

This paper belongs to a Regular Issue.

© 2022, the Authors. This article is published in open access under the terms and conditions of the Creative Commons Attribution (CC BY) license (http://creativecommons.org/licenses/by/4.0/).

Abstract

The paper is concerned with (i) the hydrothermal synthesis of hydrous zirconium dioxide (HZD) bearing analcime (HZD–ANA, zirconia-analcime) and (ii) its sorption properties with respect to Cs^+ and Sr^{2+}. The HZD–ANA particles were synthesized from coal fly ash cenospheres composed of aluminosilicate glass with $(SiO_2/Al_2O_3)_{wt.}$=3.1 and characterized by PXRD, SEM-EDS, STA, and low-temperature N_2 adsorption. The non-radioactive simulant solutions of different acidity (pH = 2–10) and Cs^+/Sr^{2+} content (0.5–50.0 mg/L) were used in the work. The effect of synthesis conditions on the HZD–ANA particle size, zirconia content and localization as well as the sorption behavior with respect to Cs^+ and Sr^{2+} (capacity, K_D) were clarified. It was found that the small-sized HZD–ANA composites surpasses the Zr-free analcime and large-sized HZD–ANA material in the Cs^+ and Sr^{2+} sorption parameters (K_D ~ 10^4–10^6 mL/g). The conditions to synthesize the zirconia-analcime composite of the highly enhanced sorption ability with respect to Sr^{2+} (K_D ~ 10^6 mL/g) were determined. The high-temperature solid-phase re-crystallization of Cs^+/Sr^{2+}-exchanged HZD–ANA composites was shown to occur at 1000 °C, resulting in a polyphase system based on nepheline, tetragonal ZrO_2, and glass phase.

Keywords

cenospheres
hydrothermal synthesis
zirconia-analcime composite
Cs(I) and Sr(II) sorption
radioactive waste

Received: 10.10.22
Revised: 04.11.22
Accepted: 05.11.22
Available online: 10.11.22

1. Introduction

The increased role of inorganic ion exchangers for treatment of radioactive waste solutions, both in nuclear power production and fuel reprocessing plants, is widely recognized [1, 2]. The sorption technologies being developed are aimed, first of all, at separation of heat-emitting fission products, such as ^{137}Cs ($T_{1/2}$ ~ 30 years) and ^{90}Sr ($T_{1/2}$ ~ 29 years) [3, 4], and long-lived actinides, e.g., Am (III), Cm (III), U (IV), Pu (IV) [5, 6]. In the context of the ultimate disposal of radioactive waste, the thermally treated inorganic ion exchangers loaded with radionuclides can function as primary mineral-like containment media in a multibarrier geological disposal system [1, 7].

From the point of view of radioactive waste minimization and reduction of a number of separation stages utilized, sorption technologies that simultaneously separate two or more radionuclides are of the greatest interest as compared with technologies that separate only one element. The management of different radionuclides together results in a single product, in which sorbed cations can accommodate in the only phase [8, 9] or be partitioned between several phases [10].

The last immobilization option can be implemented using composite sorbents based on the components differentiated by the affinity to certain radionuclides. Some composite sorbents for co-sorption of different cations, for example, alginate-encapsulated graphene oxide-layered double hydroxide beads [11], Al_2O_3–ZrO_2–CeO_2 composite material [12], poly-condensed feldspar and perlite-based sorbents [13], nickel-potassium ferrocyanide supported by hydrated titanium and zirconium dioxides [14], silica/ferrocyanide composite [15], synthetic nanocopper ferrocyanide-SiO_2 materials [16], nano composite materials from biomass waste [17] were reported.

Great capabilities for selective separation of metal cations are inherent to zeolites, which are framework aluminosilicates with an open microporosity [18, 19]. The size of pore entrances imparts a molecular/ion sieve property to zeolites. In particular, analcime (ANA) having the minimal pore entrances (d = 2.6 Å) compared to other zeolites displays an affinity towards well-proportioned cations of actinides, lanthanides, and heavy metals [20–22]. At the same time, due to the ion sieving effect, analcime has a poor Cs^+ and Sr^{2+} sorption capacity at 25 °C [23] but is capable to trap these cations under hydrothermal conditions at 250–300 °C [24].

The prospective single-phase ceramics proposed for ''minor'' actinide isolation are based on Zr-bearing mineral-like host phases including zircon, zirconia, zirconates, etc. [25, 26]. To implement the sorption approach to actinide immobilization, the Zr-based ion exchangers as precursors of Zr-bearing phases are to be used. The sorbent-precursor must be thermodynamically metastable to undergo the phase transformation in relatively mild conditions. High sorption ability and a developed porosity also facilitate crystallization of the sorbent due to the homogeneous distribution of target radionuclides in the sorbent structure. These properties are inherent to the microporous/layered ion exchange materials synthesized under mild hydrothermal treatment at 100–200 °C and autogenic pressure [27, 28]. The methods to synthesize hydrothermally nano-zirconia, zirconium incorporated micro/mesoporous silica, and zirconia-based nanocomposites were also reported [29–31].

Recently, the analcime based composite materials with hydrous zirconium dioxide (HZD) species embedded in a zeolite analcime body (HZD-ANA) were synthesized hydrothermally in an alkaline media using coal fly ash cenospheres as a Si and Al source and zirconium citrate, ammonium complex, as a Zr source [22, 32]. Variation of the synthesis conditions enables producing small-sized and large-sized ZrO_2-analcime crystals of narrow size distributions with maxima at about 6 μm [22] and 40 μm [32], respectively.

The thermal treatment of ZrO_2-bearing analcime up to 1000 °C resulted in a powdered zirconia/nepheline/glass composite material [32] having a potential as a precursor of the chemically – mechanically –, and radiation – resistant nuclear waste form, in which sorbed actinides can accommodate in a tetragonal zirconia-based phase, and retained Cs^+ and Sr^{2+} can be hosted by aluminosilicate-based or vitreous phases [33, 34].

Evaluation of sorption properties of the small-sized HZD–ANA particles with respect to Nd^{3+}, taken as an imitator of actinides (III), demonstrated that the material traps Nd^{3+} cations from diluted solutions with a distribution coefficient of about 10^5 mL/g and efficiency of up to 99.6% [22]. The Nd^{3+} sorption parameters obtained for HZD–ANA are comparable with ones determined for pure analcime.

This fact testifies that, for the most part, analcime but not zirconia is responsible for Nd^{3+} sorption on the HZD–ANA composite. As for the Zr-bearing component, zirconia in a hydrous form is an effective ion exchanger with respect to both anions and cations, including cesium and strontium [2, 35–37]. So, the HZD–ANA material is expected to display the sorption properties also towards the Cs^+ and Sr^{2+} cations.

The present paper is aimed at (i) the hydrothermal synthesis of hydrous zirconia bearing analcime under varied conditions, (ii) the evaluation of its sorption properties with respect to Cs^+ and Sr^{2+} as imitators of radionuclides ^{137}Cs and ^{90}Sr, and (iii) the demonstration of possibility to immobilize the sorbed cations of different nature in a single solid. The non-radioactive simulant solutions of different acidity (pH = 2–10) and Cs^+/Sr^{2+} contents being close to the compositions of the actual radioactive wastewater were used in the work.

2. Experimental

2.1 Chemicals and materials

The chemicals (sodium hydroxide; zirconium citrate, ammonium complex) used in this work were of reagent grade quality. They were obtained from the commercial supplier (OOO "Reactiv", Russia) and used without further purification.

The cenosphere material (marked further as $(SiO_2–Al_2O_3)_{glass}$) was a product of separation of a coal fly ash cenosphere concentrate resulted from combustion of Kuznetsk coal (Russia) [38, 39]. The chemical and phase compositions (wt.%) of the initial cenosphere fraction were as follows: SiO_2 – 67.6, Al_2O_3 – 21.0, Fe_2O_3 – 3.2, $CaO+MgO+Na_2O+K_2O$ – 7.7; quartz – 3.4, mullite – 0.8, calcite – 0.5, glass phase – 95.4; $(SiO_2/Al_2O_3)_{glass}$ – 3.1. The micrographs of the cenosphere globules are given in Figure 1.

2.2 Synthetic procedures

The small-sized zirconia bearing analcime was synthesized in the $ZrC_6H_7O_7NH_4–NaOH–H_2O–(SiO_2–Al_2O_3)_{glass}$ system of the 1.0 SiO_2/0.18 Al_2O_3/0.89 Na_2O/0.15 ZrO_2/65 H_2O molar composition using zirconium-ammonium citrate as a Zr source and cenospheres as a Si and Al source. The reaction mixture was hydrothermally treated in a Teflon-lined stainless-steel autoclave ("Beluga", Premex AG Switzerland) at 150 °C and autogenoius pressure for 48–96 h applying two stirring modes. The first one is based on the permanent stirring of the reaction mixture in the horizontal plane at a rate of 50 rpm for 48 h (the sample is denoted as SS-HZD-ANA-50). Another option is the alternate stirring in the horizontal plane at a rate of 30 rpm, under which the agitation for 30 min alternated with the two-hour non-stirring regime for 96 h (the sample is denoted as SS–HZD–ANA–30).

The solid products were separated by filtration and washed with distilled water, followed by centrifuging the suspension, separation of a sediment, and drying at 65 °C. The subsequent separation of the sediment by particle sizes was done using a sieve with an aperture of 36 μm. To remove free zirconium dioxide, the product fractions <36 μm were put into water and treated by an ultrasonic source (Cole-Parmer Instruments CPX-750, USA) for 30 min. The sediments were separated by decantation and dried at 65 °C.

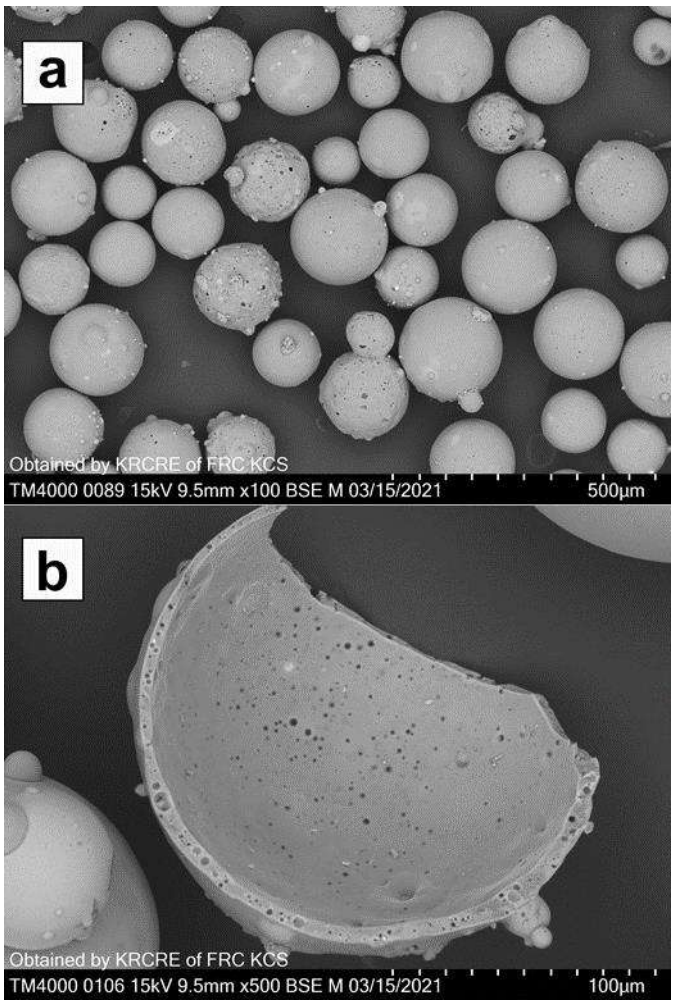

Figure 1 SEM images of initial cenospheres: total view (a); broken globule (b).

The large-sized (~40 μm) zirconia bearing analcime was prepared as described in [32] applying the agitation procedure based on rotation of the autoclave in a vertical plane at a rate of 30 rpm (the sample is denoted as LS–HZD–ANA–30).

Small-sized Zr free analcime was synthesized in the $NaOH–H_2O–(SiO_2–Al_2O_3)_{glass}$ system of the 1.0 SiO_2/0.18 Al_2O_3/0.89 Na_2O/65 molar composition under the same hydrothermal conditions (150 °C, 48 h) applying the permanent stirring of the reaction mixture in the horizontal plane at a rate of 50 rpm as described in [40] (the sample is denoted as SS–ANA–50). The solid product was washed with distilled water followed by filtration and drying at 80 °C.

2.3 Sorption experiments

Batch sorption experiments were performed upon contacting the specimen (0.0500±0.0005 g) with $CsNO_3$ or $Sr(NO_3)_2$ solution of 0.5–50.0 mg/L Cs^+/Sr^{2+} at agitation and ambient temperature (V = 40 mL; τ = 24 h). Then the solid and liquid phases were separated by filtration and Cs^+/Sr^{2+} equilibrium concentrations in the filtrate solutions were measured by flame atomic absorption spectroscopy (AAS) (AAS-30, Carl Zeiss, Germany) and, in the case of the metal content being below an AAS detection limit, inductively coupled plasma mass spectrometry (ICP-MS) (XSeries II, Thermo Scientific, USA).

The equilibrium Cs^+/Sr^{2+} concentrations in the solid phase (Q_e, mg/g) were determined as $Q_e = (C_o–C_e)\cdot V/m$, where C_o is the initial metal concentration in the liquid phase, mg/L; C_e is the equilibrium Cs^+/Sr^{2+} concentration in the liquid phase, mg/L; V is the volume of solution, L; m is the mass of the sample, g.

The experimental sorption data were plotted as $Q_e = f(C_e)$ and fitted by the Langmuir equation:

$$Q_e = a_m \cdot \frac{b \cdot C_e}{(1 + C_e)}, \quad (1)$$

where a_m is the maximum sorption capacity of the solid, mg/g; b is the Langmuir constant, L/mg; C_e is the Cs^+/Sr^{2+} equilibrium solution concentration, mg/L.

The distribution coefficient values ($K_D = Q_e/C_e$, mL/g) were determined for the region of low equilibrium concentrations (C_e < 1 mg/L).

2.4 Characterization techniques

Chemical composition of the cenosphere fraction was determined according to State Standard (GOST) No. 5382-2019 [41].

Powder X-ray diffraction (PXRD) data were collected on a DRON-3 (Russia) and a PANalytical X'Pert PRO (Netherlands) diffractometers using the Cu Kα radiation over the 2θ range of 12–120 °. The samples were prepared by grinding with octane in an agate mortar and packed into a flat sample holder for the PXRD measurements in the Bragg-Brentano geometry. The crystallographic data base JCPDS-ICDD PDF-2 Release 2004 and the software PhasanX 2.0 were used to process the PXRD patterns.

The morphologies of materials under study were identified by the scanning electron microscopy (SEM) using a TM-3000 and a TM-4000 (Hitachi, Japan) instruments. To identify the elemental composition of sample materials, energy dispersive X-ray spectroscopy (EDS or EDX) analysis was performed using the TM-3000 microscope equipped with the Bruker microanalysis system including an energy-dispersive X-ray spectrometer with an XFlash 430 H detector and QUANTAX 70 software. The analysis was carried out at an accelerating voltage of 15 kV in a mapping mode. The data accumulation time was 10 min.

The synchronic thermal analysis (STA) was performed on a STA Jupiter 449C device (Netzsch, Germany) under a dynamic argon-oxygen atmosphere (20% O_2, 50 ml/min total flow rate). Platinum crucibles with perforated lids were used. The measurement procedure consisted of a temperature stabilization segment (30 min at 40 °C) and a dynamic segment at a heating rate of 10 °/min. Qualitative composition of a gas phase was evaluated on the basis of the ion intensity change with m/z = 18 (H_2O).

The specific surface area (SSA, m^2/g) of the ANA-based materials was evaluated by the Brunauer-Emmett-Teller (BET) method [42] on the basis of nitrogen adsorption isotherm measurements at 77 K using a Nova 3200e analyzer (Quantachrome Instruments, USA) and NovaWin software.

3. Results and discussion

3.1 Morphology and composition of solid products

As it follows from Table 1, the single crystal phase identified by PXRD in all the solid products is cubic analcime (ANA), $NaAlSi_2O_6{\cdot}H_2O$ (ICDD #01–070–1575). The PXRD peaks of zirconium phases were not observed for the Zr bearing systems. This fact gives reason to assume that Zr-containing matter is essentially amorphous in the sample.

By the SEM data (Figure 2–6), crystals of an icositetrahedron habit typical of analcime [43] are visualized on all images. However, some differences in the particle morphology and analcime crystal sizes are clearly evident for solids resulted from the Zr-free and Zr-containing reaction mixtures. So, in the $Na_2O–H_2O–(SiO_2–Al_2O_3)_{glass}$ system the analcime crystals of 3–10 μm in size are attached to an unconverted glass support, forming the hollow polycrystalline analcime microspheres (Figure 2). In the presence of zirconium, the loose analcime crystals of a narrow size distribution (5–10 μm) are formed (Figure 3, 4), the analcime-like particles being the only product in the reaction mixtures.

The effect of the synthesis operation (autoclave type, agitation mode) was manifested to the greatest extent in the size of the formed particles. Figure 3 shows the large-sized zirconium-bearing analcime crystals with the size distribution maximum of about 40 μm (Figure 3a, Table 1), which were produced under rotation of the autoclave in a vertical plane and described in detail in the earlier work [32].

The zirconia inclusions in the bulk of analcime crystals with an average Zr content of 4.8 wt.% was supported in [32] by the SEM-EDS measurements over analcime crystal cross-sections and X-ray photoelectron spectroscopy.

Zirconia species are also visible as contrast white spots on facets of analcime icositetrahedra (Figure 3b, 3c) giving the Zr content of about 5 wt.% (Figure 3d). The most probable state of zirconium occurred in Zr-bearing analcime is amorphous zirconia. There is no free zirconia matter on the crystal surfaces and between analcime particles (Figure 3a). The absence of an unbound porous material mixed with analcime is supported by the measurements of the low-temperature N_2 adsorption, which was extremely small due to the inaccessibility of the analcime microporous structure (D = 0.26 nm) for penetration of nitrogen molecules with a kinetic diameter of 0.37 nm [18].

As for the small-sized Zr-analcimes synthesized in the autoclave applying the stirring in a horizontal plane, the aggregated zirconia species cover the crystal surfaces as a free porous matter (Figure 4) providing the rather high specific surface area – 30–40 $m^2{\cdot}g^{-1}$ (Table 1).

The enhanced SSA of the Zr-free SS-ANA-50 is likely to be due to the porosity of residual leached glass and micro/meso-sized voids between analcime crystals fixed on glass. The main difference between two small-sized Zr-analcimes is revealed in the Zr content on the crystal surface (Figure 4e, 4f). The analcime particles synthesized at the alternate stirring are characterized by the greater Zr content than zirconia-analcime resulted from the synthesis at the permanent agitation.

One can see in Figure 5 that the analcime particles entering the SS–HZD–ANA–30 display the inhomogenious zirconia covering with variation of the Zr content in the range of 8–14 wt.%. Additional agglomerates of an irregular form containing Zr species together with glass residues are also a part of this solid product.

Table 1 Composition, specific surface area and crystal size of the solid products.

Sample	Main crystal phase	SSA, $m^2{\cdot}g^{-1}$	Zr content, wt.%	Crystal size, μm
SS–ANA–50*	Cubic (*Ia*–3*d*) analcime $NaAlSi_2O_6{\cdot}H_2O$	36	–	2–7
SS–HZD–ANA–50		30	4–5	5–10
SS–HZD–ANA–30		39	8–13	7–10
LS–HZD–ANA–30		n.d.**	5–7	20–50/41***

*glass-supported analcime;
** not determined;
*** crystal size distribution maximum.

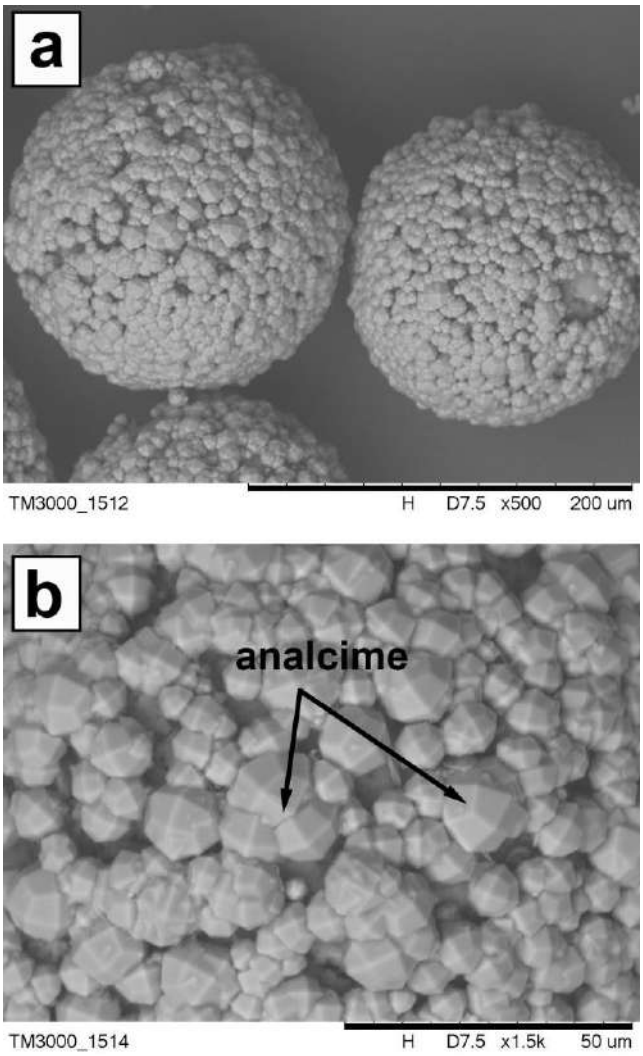

Figure 2 SEM images of Zr-free devitrified cenospheres resulted from the $NaOH–H_2O–(SiO_2–Al_2O_3)_{glass}$ system: total view of the microsphere product (a); glass-supported analcime (b).

In turn, the synthesis carried out at the permanent agitation resulted in predominantly pure zirconia-analcime with the lower content of zirconia deposition (4–7 wt.% Zr) (Figure 6). The SSA value for SS–HZD–ANA–50 is, reasonably, by one and a half time lower than the SSA for the SS–HZD–ANA–30 sample (Table 1).

Thus, the revealed features of particle morphology, zirconia occurrence form and content in the solid products are expected to affect their retention ability with respect to Cs^+ and Sr^{2+}.

3.2 Sorption behavior to Cs(I) and Sr(II) of the zirconia-analcime composites

The sorption ability of the zirconia-analcime composites with respect to Cs^+ and Sr^{2+} was evaluated by measuring the equilibrium sorption capacity at different concentrations of metal cations in solutions and pH. Figure 7 show the experimental values of Cs^+ and Sr^{2+} sorption at pH = 6 as well as the Cs^+ and Sr^{2+} sorption isotherms based on the Langmuir model for SS–ANA–50 (Figure 7a) and LS–HZD–ANA–30 (Figure 7b).

It was revealed that the Zr-free analcime bearing solid exhibits the expected poor Cs^+ and Sr^{2+} sorption capacities (Figure 7a, Table 2) because of the ion-sieve effect [18].

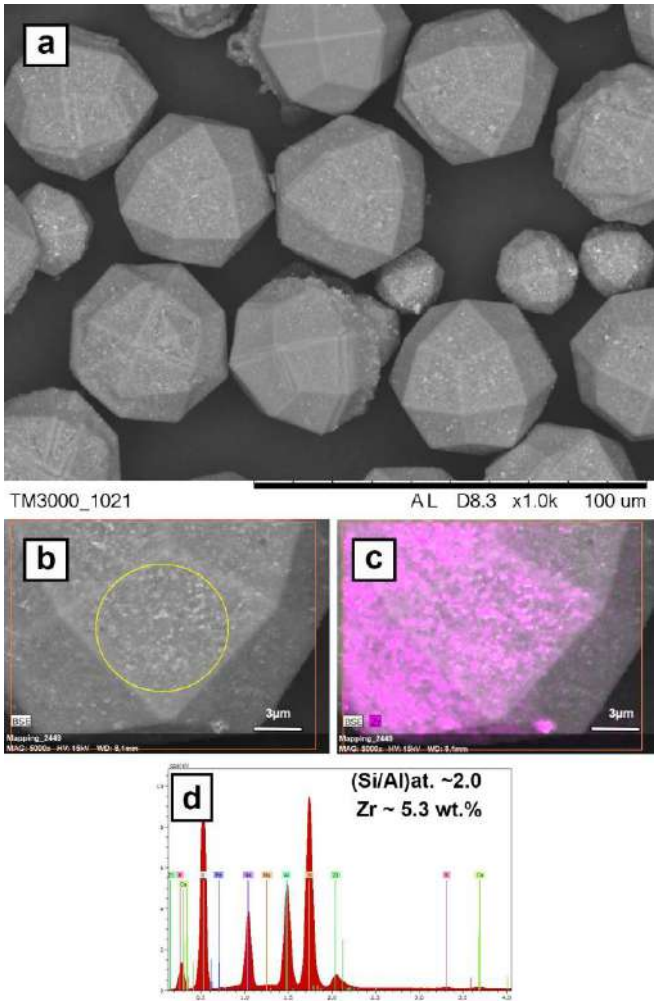

Figure 3 SEM (a) and BSE (b, c) images of LS-HZD-ANA-30 particles; EDX spectrum (d) of the marked crystal part (b) and associated Zr distribution map (c).

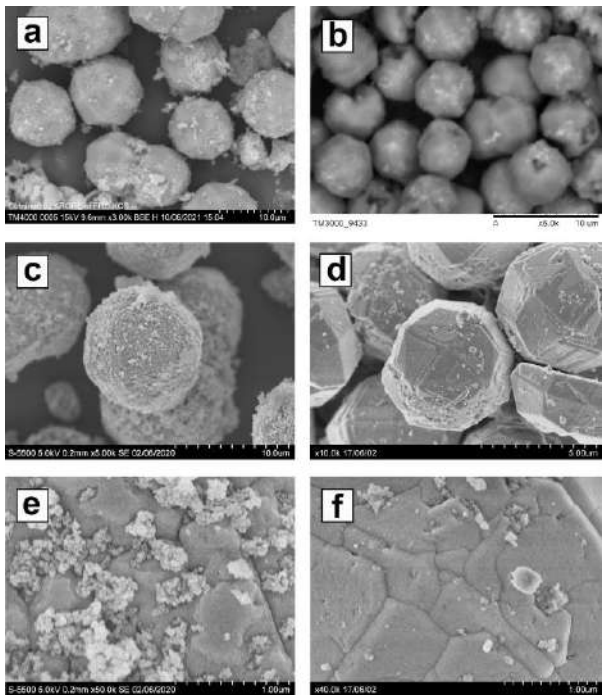

Figure 4 SEM images of small-sized HZD-analcime crystals prepared at different agitation regimes: SS–HZD–ANA–30 (a, c, e); SS–HZD–ANA–50 (b, d, f).

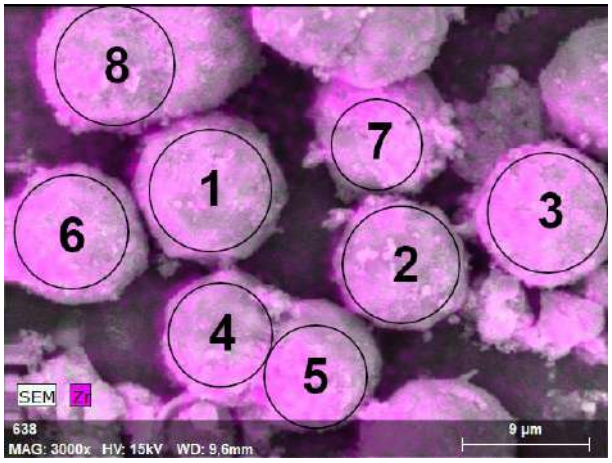

Figure 5 The Zr distribution map for SS–HZD–ANA–30 particles of the following Zr content (wt.%): 1 – 8.8; 2 – 8.5; 3 – 13.0; 4 – 8.8; 5 – 13.6; 6 – 11.2; 7 – 12.2.

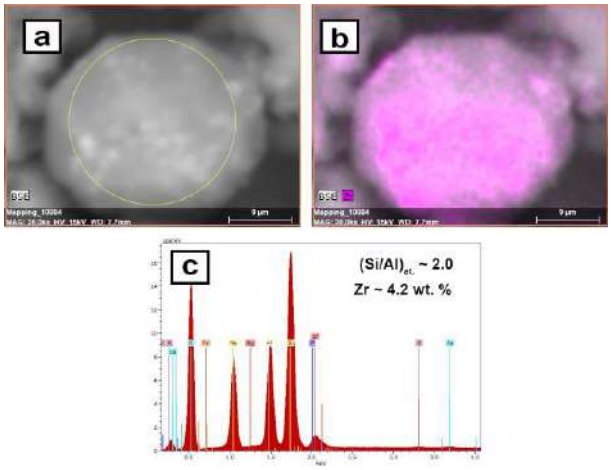

Figure 6 BSE images of a SS–HZD–ANA–50 crystal (a, b); EDX spectrum (c) of the marked crystal part (a) and associated Zr distribution map (b).

The sorption behavior of the large-sized zirconia-analcime composite is slightly better (Figure 7 b, Table 2), which is most likely due to embedded zirconia being partially available on the particle surface.

It is notable that the $Q_e = f(C_e)$ dependences for Sr^{2+} sorption on SS–HZD–ANA–30 are linear in the whole region of applied Sr^{2+} concentrations and pH, giving the K_D of up to 10^6 mL/g (Figure 8a–c). Such high Sr^{2+} sorption parameters of the small-sized zirconia-analcime composites are comparable with those for the known specific Sr^{2+} sorbents, such as hydrated antimony pentoxide [44, 45], titano- and zirconosilicates [46, 47]. A number of distribution coefficients for Cs^+ and Sr^{2+} sorption for different inorganic sorbents produced in Russia [48] are given in Table 3.

It can be seen that in near neutral solutions hydrated zirconium dioxide (Termoxide 3K) displays the higher K_D value ($3.5 \cdot 10^4$ mL/g) for the Sr^{2+} sorption than K_D for the Cs^+ sorption.

The lower K_D for the Cs^+ sorption is observed also in the case of SS–HZD–ANA–30 (Tables 2, 3). The enhanced K_D at pH ≥ 6 is the characteristic feature of amphoteric oxides, such as hydrated zirconia, operating as a cation exchanger in alkaline and neutral solutions [49]. This is also in good agreement with the zirconia content and accessibility on the analcime surface in both samples, supporting the determining role of hydrated zirconia in the Cs^+ and Sr^{2+} sorption behavior of the zirconia-analcime composites. At the same time, due to the dissolution of cenosphere's aluminosilicate glass in the alkaline reaction medium, the formation of zirconium silicate cannot be excluded. Therefore, the marked Cs^+ and Sr^{2+} sorption in acid media (Figure 8a, d) can be associated with the existence of additional binding centers, such as zirconium silicate reported as a cation exchanger [50].

Table 2 Parameters of the Langmuir equation and distribution coefficients for Cs^+ and Sr^{2+} sorption on Zr-free and Zr-bearing analcime solids.

Sample	pH	Cation	a_m, mg/g	b, L/mg	K_D, mL/g
SS–ANA–50	6	Cs^+	24.3	0.03	$9.0 \cdot 10^3$
		Sr^{2+}	15.7	0.17	$4.7 \cdot 10^3$
LS–HZD–ANA–30	6	Cs^+	30.5	0.06	$7.0 \cdot 10^3$
		Sr^{2+}	15.9	0.77	$5.0 \cdot 10^4$
SS–HZD–ANA–30	2	Cs^+	66.5	0.05	$4.8 \cdot 10^3$
		Sr^{2+}	n.d.	n.d.	$2.8 \cdot 10^3$
	6	Cs^+	39.7	0.69	$8.1 \cdot 10^4$
		Sr^{2+}	n.d.	n.d.	$1.3 \cdot 10^6$
	10	Cs^+	36.0	0.48	$5.2 \cdot 10^4$
		Sr^{2+}	n.d.	n.d.	$2.5 \cdot 10^6$
SS–HZD–ANA–50	2	Cs^+	26.9	0.11	$2.5 \cdot 10^3$
		Sr^{2+}	n.d.	n.d.	$3.0 \cdot 10^3$
	6	Cs^+	12.9	0.28	$3.6 \cdot 10^4$
		Sr^{2+}	9.3	4.2	$6.0 \cdot 10^4$
	10	Cs^+	31.5	0.43	$2.7 \cdot 10^4$
		Sr^{2+}	36.4	0.75	$2.7 \cdot 10^5$

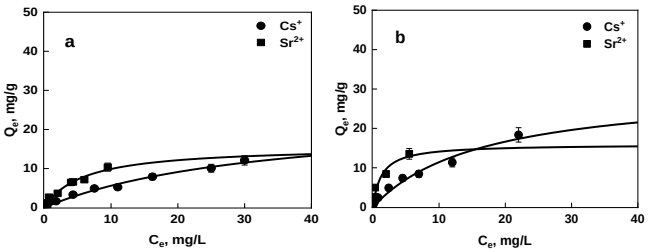

Figure 7 The Cs^+ and Sr^{2+} sorption isotherms for SS–ANA–50 (a) and LS–HZD–ANA–30 (b) at pH = 6: (points – experiment, lines – Langmuir model).

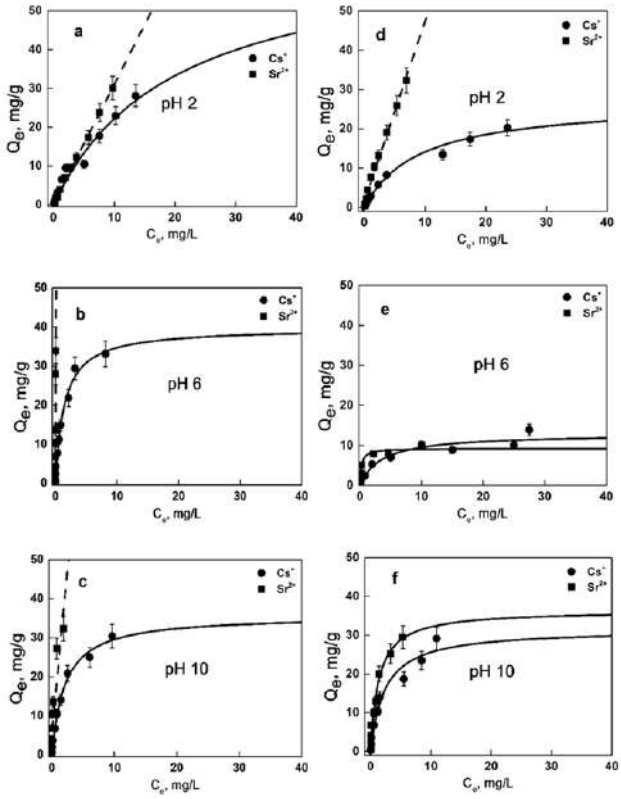

Figure 8 The Cs^+ and Sr^{2+} sorption isotherms for ZrO_2-analcime composites at different pH: SS–HZD–ANA–30 (a–c), SS–HZD–ANA–50 (d–f): (points – experiment, solid lines – Langmuir model, dashed lines – linear approximations of experimental points as a guide toeyes).

Table 3 Distribution coefficients (K_D) for Cs^+ and Sr^{2+} sorption on different inorganic sorbents in 0.1 mol/L $NaNO_3$, pH = 5–6 [48].

Sorbent	K_D, mL/g	
	Cs^+	Sr^{2+}
Natural zeolite clinoptilolite	1800	310
Bentonite clay	$1.9 \cdot 10^4$	110
Synthetic zeolite NaA	8900	$8.5 \cdot 10^4$
Synthetic zeolite NaX	1800	7900
Hydrated zirconium dioxide (Termoxide 3K)	150	$3.5 \cdot 10^4$
Zirconium phosphate (Termoxide 3A)	1800	326
Sodium titanosilicate (TiSi)	$1.9 \cdot 10^5$	$3.0 \cdot 10^4$
Nickel ferrocyanide/Hydrated zirconium dioxide (Termoxide 35)	$1.2 \cdot 10^5$	–
Nickel ferrocyanide/Silica gel	$8.4 \cdot 10^4$	–
Hydrated zirconium dioxide/Analcime (SS–HZD–ANA–30) (this work)*	$8.1 \cdot 10^4$	$1.3 \cdot 10^6$

* pH = 6, no added $NaNO_3$

3.3 Thermochemical conversion of zirconia-analcime composites loaded with Cs(I) and Sr(II)

The thermochemical conversion of the zirconia-analcime composites studied by example of the SS–HZD–ANA–30 sample loaded with Cs^+ and Sr^{2+} includes two stages (Figure 9). The first broad endothermic DSC peak with the substantial mass loss is situated at 100–400 °C and is accompanied by the simultaneous increase of intensity of m/z=18 (H_2O) ion due to the elimination of structural water from the analcime structure [32]. There are two pronounced exothermic peaks at 800–950 °C. The absence of mass change in this temperature interval suggests that the exo-effects are caused by the solid-state transformation (re-crystallization) of analcime and amorphous zirconia [51, 52].

The PXRD analysis of the zirconia-analcime composite calcined at 1000 °C revealed tetragonal zirconia (ICDD #04-005-4479) and hexagonal nepheline (ICDD #01-079-992) phases in the calcination product (Figure 1b, c), so the observed broad double peak at 800–950 °C can be assigned to the HZD and analcime (Figure 10a) phase transformation.

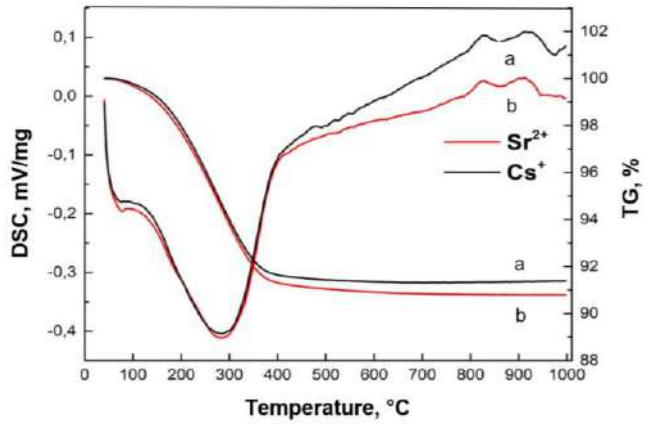

Figure 9 The TG and DSC curves for thermal conversion of the SS–HZD–ANA–30 material loaded with Cs^+ (a) and Sr^{2+} (b).

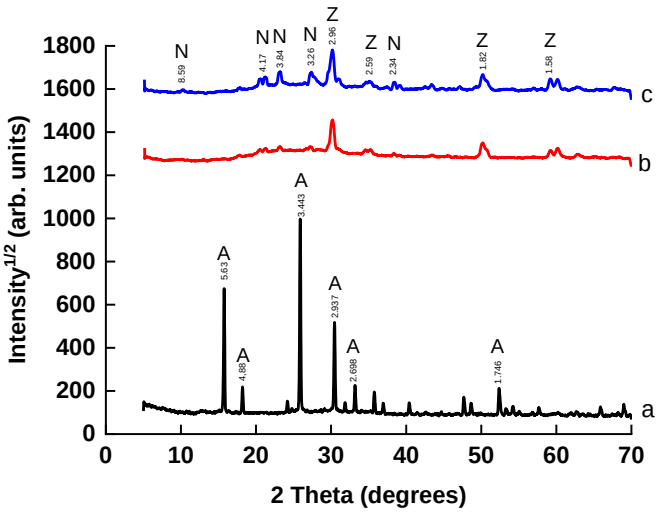

Figure 10 Powder X-ray diffraction patterns for the SS–HZD–ANA–30 (a) and solids resulted from calcination of the SS–HZD–ANA–30 loaded with sorbed Cs^+ (b) and Sr^{2+} (c) at 1000 °C: A – c-analcime (ICDD #01-070-1575), N – h-nepheline (ICDD #01-079-992), Z – t-zirconia (ICDD #04-005-4479).

The formation of tetragonal zirconia under heating is an additional evidence of the fact that amorphous zirconia that resulted from the hydrothermal synthesis is the dominant Zr-bearing matter covering the analcime surface.

Thus, the obtained data for the small-sized HZD-analcime composites loaded with Cs^+ and Sr^{2+} are in agreement with the previous STA results [32], making it possible to consider this material as the efficient Cs^+ and Sr^{2+} sorbent with a potential to be a precursor of a Zr-aluminosilicate mineral-like matrix hosting the trapped cations.

4. Conclusions

For the first time, the hydrous zirconia bearing analcime composite which demonstrated the high sorption ability to trap Cs^+ and Sr^{2+} from diluted $CsNO_3$ and $Sr(NO_3)_2$ solutions of pH = 2–10, in terms of retention capacity and distribution coefficient, was prepared under selected hydrothermal conditions starting from coal fly ash cenospheres with the $(SiO_2/Al_2O_3)_{glass}$ = 3.1. It was established that the defining role in the sorption performance to Cs^+ and Sr^{2+} belongs to the parameters such as the zirconia occurrence form, its content and the localization in the HZD–ANA particle as well as the particle size. The conditions for the synthesis of the zirconia-analcime with a highly enhanced sorption ability regarding Sr^{2+} (K_D ~10^6 mL/g) were determined.

Based on the previous knowledge together with the data obtained, the HZD-analcime composite can be considered as a sorbent targeted at both Cs^+/Sr^{2+} (due to HZD) and Ln^{3+} (due to analcime), which can simultaneously immobilize two or more radionuclides in the single product under heating with partitioning the sorbed cations between several phases – Cs^+/Sr^{2+} in the aluminosilicate phases (e.g., nepheline) and Ln^{3+}/An^{3+} in the Zr-phases (in this case, zirconia). The further testing of the sorbent on simulant waste solutions and real radioactive waste is a necessary step to confirm its effectiveness.

Supplementary materials

No supplementary materials are available.

Funding

This research was funded by Ministry of Science and Higher Education of the Russian Federation (Budget Project No. 0287-2021-0013 for the Institute of Chemistry and Chemical Technology SB RAS). The reported study was conducted by using the equipment of Krasnoyarsk Regional Research Equipment Centre of SB RAS for SEM-EDS, PXRD and AAS analyses and Siberian Federal University for STA, PXRD and ICP-MS analyses.

Acknowledgments

The authors acknowledge G.N. Bondarenko and L.A. Solovyov for performing the PXRD, S.N. Vereshchagin for the

STA, E.V. Mazurova for the SEM-EDS, O.A. Levitskaya and V.R. Kuzik for the AAS analysis.

Author contributions

Conceptualization: V.T.A., A.A.G.
Data curation: K.E.A.
Formal Analysis: K.E.A., B.O.V.
Funding acquisition: V.T.A., A.A.G.
Investigation: K.E.A., B.O.V.
Methodology: V.T.A., A.A.G.
Project administration: A.A.G.
Resources: K.E.A., B.O.V.
Software: K.E.A., B.O.V.
Supervision: A.A.G.
Writing – original draft: V.T.A.
Writing – review & editing: V.T.A.

Conflict of interest

The authors declare no conflict of interest.

Additional information

Author IDs:

Tatiana A. Vereshchagina, Scopus ID 670142870;
Ekaterina A. Kutikhina, Scopus ID 24399263000;
Olga V. Buyko, Scopus ID 26026599100;
Alexander G. Anshits, Scopus ID 57200009289.

Websites:

Institute of Chemistry and Chemical Technology SB RAS, Federal Research Center "Krasnoyarsk Science Center SB RAS", https://ksc.krasn.ru;

Siberian Federal University, https://www.sfu-kras.ru.

References

1. International Atomic Energy Agency, Application of Ion Exchange Processes for the Treatment of Radioactive Waste and Management of Spent Ion Exchangers. Tech. Rep. Ser. No. 408. Vienna: IAEA; 2002. 124 p.
2. Clearfield A. Inorganic ion exchangers, past, present, and future. Solvent Extr Ion Exch. 2000;18:655–678. doi:10.1080/07366290008934702
3. El-Kamash AM. Evaluation of zeolite A for the sorptive removal of Cs^+ and Sr^{2+} ions from aqueous solutions using batch and fixed bed column operations. J Hazard Mater. 2008;151:432–445. doi:10.1016/j.jhazmat.2007.06.009
4. Figueiredo BR, Cardoso SP, Portugal I, Rocha J, Silva CM, Inorganic ion exchangers for cesium removal from radioactive wastewater. Separ Purif Rev. 2018;47:306–336. doi:10.1080/15422119.2017.1392974
5. Peters TB, Barnes MJ, Hobbs DT, Walker DD, Fondeur FF, Norato MA, Fink SD, Pulmano RL. Strontium and actinide separations from high level nuclear waste solutions using monosodium titanate 2. Actual Waste Testing. Separ Sci Technol. 2006;41:2409–2427. doi:10.1080/01496390600742963
6. Pichot E, Dacheux N, Brandel V, Genet M. Investigation of $^{137}Cs^+$, $^{85}Sr^{2+}$ and $^{241}Am^{3+}$ ion exchange on thorium phosphate hydrogenphosphate and their immobilization in the thorium phosphate diphosphate. New J Chem. 2000;24:1017–1023. doi:10.1039/B006022O
7. Saeb S, Patchet SJ. Radioactive Waste Disposal (Geology). Editor(s): Robert A. Meyers, Encyclopedia of Physical Science and Technology (3nd ed.). Moscow: Academic Press; 2003. P. 633–641. doi:10.1016/B0-12-227410-5/00641-4
8. Vereshchagina TA, Fomenko EV, Vasilieva NG, Solovyov LA, Vereshchagin SN, Bazarova ZG, Anshits AG. A novel layered zirconium molybdate as a precursor to a ceramic zirconomolybdate host for lanthanide bearing radioactive waste. J. Mater. Chem. 2011;21:12001–12007. doi:10.1039/C1JM11202C
9. Mimura H, Akiba K, Ozawa M. Preparation of ceramic solid forms immobilizing cesium and/or strontium and evaluation of their physical and chemical properties. In: Proc. Inter. Conf. Nuclear Energy for New Europe; 2002 Sep 9–12; Kranjska Gora, Slovenia. p. 62640.
10. Dosch RG. Ceramic from ion exchangers: an approach to nuclear waste solidification. Trans Amer Nucl. Soc. 1975;22:355–357.
11. Guo B, Kamura Y, Koilraj P, Sasaki K. Co-sorption of Sr^{2+} and SeO_4^{2-} as the surrogate of radionuclide by alginate-encapsulated graphene oxide-layered double hydroxide beads. Environ. Res. 2020;187:109712. doi:10.1016/j.envres.2020.109712
12. Attallah MF, Hassan HS, Youssef MA. Synthesis and sorption potential study of Al_2O_3–ZrO_2–CeO_2 composite material for removal of some radionuclides from radioactive waste effluent. Appl Radiat Isot. 2019;147:40–47. doi:10.1515/ract-2019-3221
13. Youssef MA, El-Naggar MR, Ahmed IM, Attallah MF. Batch kinetics of ^{134}Cs and $^{152+154}Eu$ radionuclides onto poly-condensed feldspar and perlite based sorbents. J. Hazard Mater. 2021;403:123945. doi:10.1016/j.jhazmat.2020.123945
14. Voronina AV, Noskova AYu, Semenishchev VS, Gupta DK. Decontamination of seawater from ^{137}Cs and ^{90}Sr radionuclides using inorganic sorbents. J Environ Radioact. 2020;217:106210. doi:10.1016/j.jenvrad.2020.106210
15. Mahmoud MR, Seliman AF. Evaluation of silica/ferrocyanide composite as a dual-function material for simultaneous removal of $^{137}Cs^+$ and $^{99}TcO_4^-$ from aqueous solutions. Appl Radiat Isot. 2014;91:141–154. doi:10.1016/j.apradiso.2014.05.021
16. Nayl AA, Ahmed IM, Abd-Elhamid AI, Aly HF, Attallah MF. Selective sorption of ^{134}Cs and ^{60}Co radioisotopes using synthetic nanocopper ferrocyanide-SiO_2 materials. Sep Purif Technol. 2020;234:116060. doi:10.1016/j.seppur.2019.116060
17. Attallah MF, Youssef MA, Imam DM. Preparation of novel nano composite materials from biomass waste and their sorptive characteristics for certain radionuclides. Radiochim Acta. 2020;108:137–149. doi:10.1515/ract-2019-3108
18. Breck DW. Zeolite Molecular Sieves: Structure, Chemistry, and Use. New York: John Wiley & Sons; 1974. 771 p.
19. Jiménez-Reyes M, Almazán-Sánchez PT, Solache-Ríosa M. Radioactive waste treatments by using zeolites. A short review. J Environ Radioact. 2021;233:106610. doi:10.1016/j.jenvrad.2021.106610
20. Rachkova NG, Taskaev AI. Immobilization of U, Ra, and Th compounds with analcime-containing rock and hydrolysis lignin. Radiochem. 2011;53:314–321. doi:10.1134/S1066362211030155
21. Hegazy EZ, Abd El Maksod IH, Abo El Enin RMM. Preparation and characterization of Ti and V modified analcime from local kaolin. Appl Clay Sci. 2010;49:149–155. doi:10.1016/j.clay.2010.04.019
22. Vereshchagina TA, Kutikhina EA, Chernykh YaYu, Fomenko EV, Mazurova EV, Vereshchagin SN, Bondarenko GN. Preparation and properties of Zr-bearing sorption materials based on coal fly ash microspheres. J Sib Fed Univ Chem. 2019;12:347–363. doi:10.17516/1998-2836-0132
23. Ames LL. Cation exchange properties of wairakite and analcime. Amer Miner. 1966;51:903–909.
24. Redkin AF, Hemley JJ. Experimental Cs and Sr sorption on analcime in rock-buffered systems at 250–300 °C and P_{sat} and the thermodynamic evaluation of mineral solubilities and

phase relations. Eur J Mineral. 2000;12:999–1014. doi:10.1127/0935-1221/2000/0012-0999
25. Trachenko K, Understanding resistance to amorphization by radiation damage. J Phys Condens Matter. 2004;16:R1491–R1515. doi:10.1088/0953-8984/16/49/R03
26. Lee WE, Ojovan MI, Stennett MC, Hyatt NC. Immobilisation of radioactive waste in glasses, glass composite materials and ceramics. Adv Appl Ceram. 2006;105:3–12. doi:10.1179/174367606X81669
27. Luca V, Griffith CS, Drabarek E, Chronis H. Tungsten bronze-based nuclear waste form ceramics. Part 1. Conversion of microporous tungstates to leach resistant ceramics. J Nucl Mater. 2006;358:139–150. doi:10.1016/j.jnucmat.2006.06.017
28. Borade RB, Clearfield A. Hydrothermal synthesis of an iron silicate with layered structure. Chem Commun. 1997:277–278. doi:10.1039/A606343H
29. Liu L, Wang S, Zhang B, Jiang G, Yang J. Supercritical hydrothermal synthesis of nano-ZrO_2: Influence of technological parameters and mechanism. J Alloys Comp. 2022;898:162878. doi:10.1016/j.jallcom.2021.162878
30. Zhang M, Sheng X, Zhang Y, Zhou Y, Zhao S, Fu X, Zhang H. Zirconium incorporated micro/mesoporous silica solid acid catalysts for alkylation of o-xylene with styrene. J Porous Mater. 2017;24:109–120. doi:10.1007/s10934-016-0243-7
31. Luo X, Wang X, Bao S, Liu X, Zhang W, Fang T. Adsorption of phosphate in water using one-step synthesized zirconium-loaded reduced graphene oxide. Sci Rep. 2016;6:39108. doi:10.1038/srep39108
32. Vereshchagina TA, Kutikhina EA, Solovyov LA, Vereshchagin SN, Mazurova EV, Chernykh YaYu, Anshits AG. Synthesis and structure of analcime and analcime-zirconia composite derived from coal fly ash cenospheres. Microporous Mesoporous Mater. 2018;258:228–235. doi:10.1016/j.micromeso.2017.09.011
33. Orlova AI, Ojovan MI. Ceramic mineral waste-forms for nuclear waste immobilization. Mater. 2019;12:2638. doi:10.3390/ma12162638
34. The National Academies Press. Waste Forms Technology and Performance: Final Report. Committee on Waste Forms Technology and Performance. National Research Council: Washington, DC, USA. 2011. 308 p. doi:10.17226/13100
35. Hamoud MA, Allan KF, Sanad WA, El-Hamouly SH, Ayoub RR. Gamma irradiation induced preparation of poly(acrylamide-itaconic acid)/zirconium hydrous oxide for removal of Cs-134 radionuclide and methylene blue. J Radioanal Nucl Chem. 2014;302:169–178. doi:10.1007/s10967-014-3206-y
36. Tel H, Altas Y, Gur F, Ugur A. Sorption kinetics of cesium on ZrO_2 and ZrO_2–SiO_2–TiO_2 microspheres. Radiochim Acta. 2010;98:215–219. doi:10.1524/ract.2010.1707
37. Venkatesan KA, Selvam GP, Rao PRV. Sorption of strontium on hydrous zirconium oxide. Sep Sci Technol. 2000;35:2343–2357. doi:10.1081/SS-100102106
38. Anshits NN, Mikhailova OA, Salanov AN, Anshits AG. Chemical composition and structure of the shell of fly ash non-perforated cenospheres produced from the combustion of the Kuznetsk coal (Russia). Fuel. 2010; 89: 1849–1862. doi:10.1016/j.fuel.2010.03.049
39. Fomenko EV, Anshits NN, Solovyov LA, Mikhaylova OA, Anshits AG. Composition and morphology of fly ash cenospheres produced from the combustion of Kuznetsk coal. Energy Fuels. 2013; 27: 5440–5448. doi:10.1021/ef400754c
40. Vereshchagina TA, Kutikhina EA, Chernykh YaYu, Solovyov LA, Zhizhaev AM, Vereshchagin SN, Anshits AG. One-step immobilization of cesium and strontium from alkaline solutions via a facile hydrothermal route. J Nucl Mater. 2018;510:243–255. doi:10.1016/j.jnucmat.2018.08.015
41. Cements and materials for cement production. Chemical analysis methods. State Standard (GOST) No. 5382–2019. Moscow: IPK, Izdatel'stvo standartov; 2002. 70 p.
42. Greg SJ, Singh KSW. Adsorption, Surface Area, and Porosity. London: Academic Press; 1982. 304 p.
43. Wise WS. Handbook of Natural Zeolites. ed. C. Colella. International Zeolite Association. Napoli, Italy, A. De Frede Edotore: Natural Zeolites Commission; 2013. 126 p.
44. Mu W, Zhang R, Li X, Xie X, Yu Q, Lv K, Wei H, Jian Y. Pyrochlore Ta-doped antimony oxide as a novel adsorbent for efficient strontium removal. RSC Adv. 2015;5:10378–10385. doi:10.1039/C4RA13992E
45. Shavinsky BM, Levchenko LM, Mitkin VN. Obtaining hydrated antimony pentoxide for the sorption of cesium and strontium ions. Chem Sustain Develop. 2010;18:663–667.
46. Popa K, Pavela CC. Radioactive wastewaters purification using titanosilicates materials: State of the art and perspectives. Desalination. 2012;293:78–86. doi:10.1016/j.desal.2012.02.027
47. Bortun AI, Bortun LN, Clearfield A. Hydrothermal synthesis of sodium zirconium silicates and characterization of their properties. Chem Mater. 1997;9:1854–1864. doi:10.1021/cm9701419
48. Milyutin VV, Nekrasova NA, Kaptakov VO. Modern sorption materials for cesium and strontium radionuclide extraction from liquid radioactive waste radioactive waste. Radioact Waste. 2020;4(13):80—89 (In Russian). doi:10 25283/2587-9707-2020-4-80-89
49. Misak NZ. Outlines of the ion exchange characteristics of hydrous oxides. Adv Colloid Interface Sci. 1994;51:29–135. doi:10.1016/0001-8686(94)80034-0
50. Amphlett CB. Inorganic Ion exchangers. New York, London: Elsevier Pub. Co; 1964. 141 p.
51. Suvorova VA, Kotel'nikov AR, Akhmedzhanova GM. Phase Transformation of Zeolites Saturated with Alkali and Alkaline-Earth Elements into Ceramic. Vestn Ross Akad Nauk Ser Earth Sci. 2002;1:20.
52. Kotel'nikov AR, Bychkov AM, Zyryanov VN, Akhmedzhanova GM, Gavlina OT. Phase Transformation of Zeolites into Feldspar as a Method for Preparing Aluminosilicate Matrices for Radionuclide Fixation. Geokhimiya. 1995;10:1527–1532.